Shelfbreak Jet Structure and Variability off New Jersey Using Ship of Opportunity Data From the CMV Oleander

JGR Oceans

RESEARCH ARTICLE
10.1029/2020JC016455

Shelfbreak Jet Structure and Variability off New Jersey Using Ship of Opportunity Data From the *CMV* Oleander

Jacob Forsyth[1,2], **Magdalena Andres**[1], **and Glen Gawarkiewicz**[1]

[1]Department of Physical Oceanography, Woods Hole Oceanographic Institution, Woods Hole, MA, USA, [2]Department of Earth, Atmospheric, and Planetary Sciences, Massachusetts Institute of Technology, Cambridge, MA, USA

Key Points:
- Shelfbreak Jet mean structure and a monthly climatology are quantified in both Eulerian and stream coordinate frameworks
- Warm Core Rings influence the position and velocity structure of the Shelfbreak Jet on the New Jersey Shelf
- The Shelfbreak Jet velocity is correlated with the temperature on the continental shelf with warm temperatures associated with a slower jet

Supporting Information:
- Supporting Information S1

Correspondence to:
J. Forsyth,
jforsyth@whoi.edu

Citation:
Forsyth, J., Andres, M., & Gawarkiewicz, G. (2020). Shelfbreak Jet structure and variability off New Jersey using ship of opportunity data from the *CMV* Oleander. *Journal of Geophysical Research: Oceans*, *125*, e2020JC016455. https://doi.org/10.1029/2020JC016455

Received 28 MAY 2020
Accepted 26 AUG 2020
Accepted article online 30 AUG 2020

Abstract Repeat measurements of velocity and temperature profiles from the Container Motor Vessel (*CMV*) Oleander provide an unprecedented look into the variability on the New Jersey Shelf and upper continental slope. Here 1362 acoustic Doppler current profiler (ADCP) velocity sections collected between 1994 and 2018 are analyzed in both Eulerian and stream coordinate reference frames to characterize the mean structure of the Shelfbreak Jet, as well as its seasonal to decadal variability. The Eulerian mean Shelfbreak Jet has a maximum jet velocity of 0.12 m s^{-1}. The maximum jet velocity peaks in April and May and reaches its minimum in July and August. In a stream coordinate framework, the jet is only identified in 61% of transects, and the mean stream coordinate Shelfbreak Jet has a maximum jet velocity of 0.32 m s^{-1}. Evidence is found that Warm Core Rings, originating from the Gulf Stream arriving in the Slope Sea adjacent to the New Jersey Shelf, shift the Shelfbreak Jet onshore of its mean position or entirely shutdown the Shelfbreak Jet's flow. At interannual timescales, variability in the Shelfbreak Jet velocity is correlated with the temperature on the New Jersey Shelf 2 months later. When considered in a stream coordinate framework, Shelfbreak Jet have decreased over the time period considered in the study.

Plain Language Summary At the shelf break off the coast of New Jersey, an intensified current exists that flows equatorward called the Shelfbreak Jet. We use 25 years of observational velocity data from 1994–2018, collected by a container ship, to study this jet. Averaging the data over the whole time period shows a concentrated jet over the shelf break, and we calculate the velocity, size, and transport of this jet. We analyze every transect of velocity data that we have and check if the Shelfbreak Jet is present during this time. The jet only exists in 61% of our transects. We average the velocities when the Shelfbreak Jet is present and characterize the velocity structure of the mean Shelfbreak Jet. The jet moves onshore and offshore over time. We find that during time periods when the jet is moved onshore, as well as when the jet does not exist in our transects, it is in part due to Warm Core Rings. A Warm Core Ring is a northward excursion of warm salty Gulf Stream water that is isolated from the Gulf Stream. Additionally, we find that the velocity of the Shelfbreak Jet is related to the temperature on the New Jersey Shelf.

1. Introduction

The Middle Atlantic Bight (MAB) Shelfbreak Jet is an equatorward flowing jet, concentrated over the shelf break. This Shelfbreak Jet is part of a coastal current system, flowing from the Labrador Sea, along the east coast of North America at the edge of the shelf, until it reaches the Gulf Stream at Cape Hatteras. From north to south, the Shelfbreak Jet transport declines from a few Sverdrups in the Labrador Sea, to a fraction of a Sverdrup on the MAB (Fratantoni & Pickart, 2007; Loder et al., 1998). The mean circulation of this coastal current has been studied as both a continuous feature, and at specific regional sites. Most commonly, hydrographic studies have documented the mean geostrophic transport using the thermal-wind equations (e.g., Fratantoni & Pickart, 2007; Linder & Gawarkiewicz, 1998).

In the MAB, the Shelfbreak Jet is typically associated with the Shelfbreak Front. This front separates the cool fresh shelf waters from the warm saltier slope water, leading to a large gradient in density. Calculations of the Shelfbreak Jet's barotropic and baroclinic components have found that roughly half of the total transport is baroclinic (Fratantoni & Pickart, 2007). The identity of the Shelfbreak Jet is not dependent on being found in the Shelfbreak Front; however, the density gradients greatly enhance the transport of the Jet.

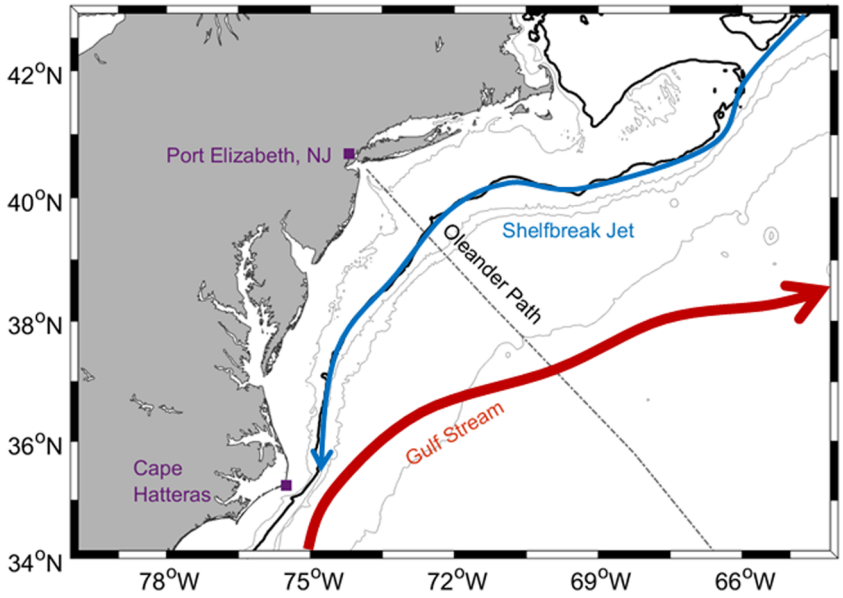

Figure 1. Map of the MAB including the locations of the Shelfbreak Jet (blue) and Gulf Stream (red). The Oleander path (gray dashed line) goes from Port Elizabeth, New Jersey, to Bermuda. Gray contours of bathymetry are shown indicating the 40-, 1,000-, 2,000-, and 4,000-m isobath, with the 100-m isobath shown in black.

The Shelfbreak Jet in the MAB has been regularly sampled since 1992 using shipboard acoustic Doppler current profilers (ADCPs) from the ship of opportunity program Container Motor Vessel (*CMV*) Oleander (Figure 1). Flagg et al. (2006) used the Oleander observations from 1992–2002 to detail the Shelfbreak Jet during time periods without Warm Core Rings present on the Oleander's route. Using these observations, they were able to study the mean structure of the Shelfbreak Jet. With over 200 transects, Flagg et al. (2006) also quantified the seasonal to interannual variability.

The impact of Warm Core Rings on the Shelfbreak Jet is contested and may depend on the region and time period considered. Fratantoni and Pickart (2003) found that rings were not a significant driver of variability on the New England Shelf; however, other studies have shown that Warm Core Rings are able to shift the position of the Shelfbreak Jet or even reverse the direction of the jet on the New England Shelf and MAB (Beardsley et al., 1985; Zhang & Gawarkiewicz, 2015). Not including rings to study the variability of the jet may miss a key mechanism that influences the Shelfbreak Jet, especially as more Warm Core Rings have been observed per year since 2000 in the Northwest Atlantic (Gangopadhyay et al., 2019). Since the increase in rings per year, Warm Core Rings have been a driver in some marine heat waves on the shelf (Gawarkiewicz et al., 2019).

Here we present observations from the *CMV* Oleander from 1994–2018, building on the Flagg et al. (2006) study of the Shelfbreak Jet with an additional 14 years of velocity sections, and considering sections where Warm Core Rings are present. By including all sections, we are able to establish the mean velocity structure at the shelf break and the velocity variability. Using this ADCP data also allows for a greater understanding of the spatial scales of the Shelfbreak Jet and its variability relative to the hydrographic and mooring-based studies. The 25 years of data are unprecedented in this region and allow for the study of variability on timescales previously not considered.

In the following, we describe the relevant data sets from the *CMV* Oleander and from satellites in section 2. We discuss our methodologies to create gridded and quality controlled temperature and velocity products. Within section 2, we also outline our methodology for identifying the Shelfbreak Jet. The Eulerian mean Shelfbreak Jet structure and the seasonal variability of this jet are described in section 3. We then further analyze the Shelfbreak Jet structure by creating means using a stream coordinate framework. The Shelfbreak Jet's variability is investigated by employing several conditional averaging techniques. Lastly, we relate the interannual Shelfbreak Jet variability to the temperature variability on the shelf. We present our conclusions in section 5.

2. Data and Methods

2.1. *CMV* Oleander Measurements

Since 1977, the *CMV* Oleander has taken measurements of upper-ocean properties on its weekly trips between Port Elizabeth, New Jersey, and Bermuda. Temperature profiles measured with expendable bathythermographs (XBTs), and surface temperature and salinity observations using bucket measurements, have been collected since 1977, while ocean velocity profiles from ADCPs began in late 1992. Beginning in 2000, a thermosalinograph (TSG) was used to measure the surface temperature and salinity, replacing the bucket measurements. Here we describe two gridded products that we generated from the XBT and ADCP data.

2.1.1. XBT Temperature Sections

The XBT data set was previously used in Forsyth et al. (2015). Here we report updates to the methodology from the previous work and describe the details of the final gridded product. To reduce errors from slight variations in the *CMV* Oleander track from one transit to the next, we only use data taken within 15 km of the Oleander's median path between New Jersey and Bermuda (Flagg et al., 2006). The data are then projected onto the median path. Each individual transect is gridded with 10-km horizontal resolution and 5-m vertical resolution due to the spacing of sampling, and the recording of the earlier data.

We create a monthly product from the individual XBT temperature transects, which are taken approximately 14 times a year. In months with multiple transects, we average the gridded transects within the month. If no data exist in a particular month, we use the following mapping technique to fill the gaps. First, we remove the seasonal cycle from all available gridded transects by subtracting the climatological monthly signal from each. Then we calculate the decorrelation timescale at each grid point and use these to map the temperature anomalies where we did not previously have data. Lastly, the monthly climatological signal is added back in. The final product comprises monthly gridded temperature sections spanning the New Jersey Shelf, to the northern edge of the Gulf Stream from 1977–2018. We only grid data to the north wall of the Gulf Stream as XBT data south of this are not consistently available in the earlier parts of the record.

2.1.2. ADCP Velocity Sections

Two different ADCPs have been used on the Oleander since 1992, a 150-kHz unit was used from 1992–2004, and in 2005 a 75-kHz ADCP replaced the higher frequency model. Here we examine data from 1994–2018, which comprises 808 crossings from the 150-kHz ADCP and 977 crossings from the 75-kHz unit. Data were binned at varying vertical resolutions, and at 5-min intervals, which gives a typical horizontal resolution of 2.4 km (Flagg et al., 2006). As with the XBT measurements, we only consider data that fall within 15 km of the Oleander's median path. We then apply a previously developed quality control mask (Flagg et al., 1998). While this removes most of the bad data, we apply additional quality control measures described below to further reduce errors. Using all of the ADCP data, we establish the mean bathymetry along the Oleander line (from the bottom reflections) and then remove all data that fall beneath this depth.

The 150-kHz ADCP recorded data in 4-m depth bins on the shelf, defined as shallower than the 100-m isobath, with the surface bin centered at 10 m. Offshore of the 100-m isobath, the bin resolution was 8 m with the shallowest bin centered at 20-m depth. In contrast, the 75-kHz ADCP most often recorded data onshore of the 1,000-m isobath with 8-m bins, with the surface bin centered between 20 and 22 m. Offshore of the 1,000-m isobath, the 75-kHz ADCP recorded at a 16-m bin resolution with the top bin centered at 30 m. While both ADCPs typically gathered data at the aforementioned bin sizes, the bin size and the depth of the surface bin vary between transects. Due to differences in the data acquisition settings for the two different ADCPs, and the differences in data acquisition settings within an individual transect, we divide the data based on ADCP and depth region to further quality control the data.

For each ADCP and depth region, we calculate the mean velocity and standard deviations at each depth level for horizontal and vertical velocities. Binned data with vertical velocities outside two standard deviations from the mean are removed. This primarily removes data in the surface layer where the measurements are noisy and plagued by bubble sweep down. Individual bins with horizontal velocities over two standard deviations from the mean are flagged and examined further. Flagged data are removed unless they are part of a feature, like a Warm Core Ring impinging on the shelf or a large meander of the Shelfbreak Jet, which could indeed have velocities over two standard deviations away from the time mean shelf and slope velocities. Additionally, entire transects are removed if data return is poor and inconsistent throughout the transect.

After this quality control, we have 693 150-kHz transects and 669 75-kHz transects. We then remove the barotropic tides (Egbert & Erofeeva, 2002). The 150-kHz data are gridded with 4-km horizontal and 8-m vertical resolution. For the 75-kHz data, we grid the data on a 4-km horizontal resolution, with the shallow data with 8-m vertical resolution and the deeper data on a 16-m vertical resolution. For ease of comparison, we linearly interpolate the deeper 75-kHz data onto an 8-m vertical grid. These data sets are then combined for a total of 1,362 transects of ADCP-measured horizontal velocity on a 4 km by 8 m grid from 1994–2018. The distance grid is set based on Ambrose Light, which is in New York Harbor, at the north western end of the Oleander transect (Figure 1).

In this study, we define our velocities based on the orientation of the shelf break along the median path of the Oleander line on the New Jersey Shelf. The shelf break runs in the northeast-southwest direction with the mean Shelfbreak Jet flowing to the southwest. Thus, we rotate our velocities to be in the along-shelf, or southwest direction (225°T), and cross-shelf, or southeast (135°T) direction.

2.1.3. Shelfbreak Jet Identification

In order to study the Shelfbreak Jet, we develop a method to identify the jet in a given transect. First, we identify features that could be the Shelfbreak Jet by finding all the local depth-averaged along-shelf velocity maxima within a segment of the Oleander track spanning 120 km centered at the 100-m isobath. Next, we calculate the depth-averaged velocity, the direction of the mean velocity, and the relative vorticity bracketing each velocity maximum. Here we define relative vorticity, $\zeta = \frac{\partial u}{\partial y}$, as the change in along-shelf flow in the cross-shelf direction, which is in the direction of the Oleander transect. Along-shelf gradients in the cross-shelf flow tend to be much weaker in this region, and thus, we use this simplified form of relative vorticity. If TSG data exist during the ADCP transect (during 473 of the ADCP transects), we additionally consider the salinity, and the cross-shelf salinity gradient.

Our method identifies a Shelfbreak Jet and finds its position only when the following four criteria are met: (1) Maximum velocity is above 0.15 m s^{-1}, (2) the direction of the flow is predominantly along-shelf, (3) the relative vorticity on both sides of the jet is larger than the background values, and (4) the jet's along-shelf velocity decreases below 100 m. The velocity used for Criterion 1 is chosen because it is about half as strong as the core of the time-averaged Shelfbreak Jet calculated using a stream coordinate frame (Flagg et al., 2006). Requiring the identified jets to decrease in along-shelf velocity with depth prevents our method from mistaking onshore meanders of the more barotropic Slope Jet as the Shelfbreak Jet (Flagg et al., 2006). If we do not have data below 100 m, either because the water depth is shallower than 100 m or because the data deeper than 100 m were removed in the quality control, we assume Criterion 4 is satisfied.

If multiple velocity cores are identified in one transect using the above criteria, we compare the velocity cores' properties and rank them to be consistent with the observed Shelfbreak Jet identified in past research (Flagg et al., 2006; Fratantoni et al., 2001; Linder & Gawarkiewicz, 1998). The properties and highest rank of each property are, the velocity core with the highest velocity, velocity cores where the magnitude of the relative vorticity on the cyclonic side is greater than the magnitude of relative vorticity on the anticyclonic side, the velocity core that is closest in distance to the mean climatological position of the Shelfbreak Jet, and if TSG data exist for the section, the velocity core that is closest to the 34.5 isohaline which is taken to define the Shelfbreak Front (Linder & Gawarkiewicz, 1998). The velocity core that is the most consistent with past observations of the Shelfbreak Jet is then selected as the jet.

2.2. Satellite

We use satellite data to study spatial variability along the MAB and Slope Sea from 1994–2018 and to provide spatial context for the variability observed at the Oleander Line. For sea surface temperature (SST) we use National Oceanographic and Atmospheric Administration (NOAA) Optimum Interpolation (OI) $\left(\frac{1}{4}\right)^\circ$ daily SST (AVHRR only Reynolds et al., 2007). Additionally, we use daily mapped absolute dynamic topography at $\left(\frac{1}{4}\right)^\circ$ resolution, available through E.U. Copernicus Marine Environmental Monitoring Service to provide sea surface height (SSH) data, and SSH-derived geostrophic velocities.

To verify that satellite altimetry can be used to study the Shelfbreak Jet, we interpolate the mean SSH-derived geostrophic velocities calculated from SSH gradients onto the Oleander path. The maximum along-shelf velocity from satellite altimetry is 0.11 m s^{-1} and is found at the 91-m isobath. These values are similar to what we will report later as the position and maximum jet velocity of the Eulerian mean Shelfbreak Jet from the in situ ADCP measurements. The position of the jet is accurate within the satellite spatial feature

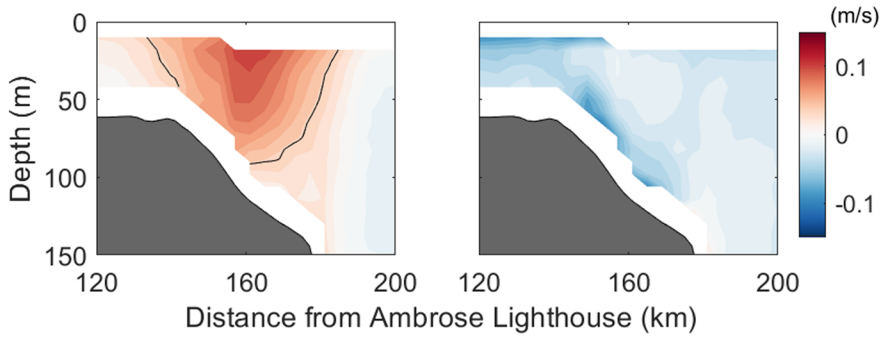

Figure 2. Eulerian mean along-shelf velocity (left column) and cross-shelf velocity (right column) from 1,362 sections. The e-folding isotach (black line) is plotted for mean along-shelf velocity.

resolution, which is approximately 40 km (Chelton et al., 2011). We find that the satellite data are able to reproduce the features we are studying, though at a much coarser scale that is still useful in providing broader spatial context.

3. Mean and Climatological Structure

3.1. Eulerian Mean Shelfbreak Jet Velocity Structure and Transport

Using all 1,362 gridded velocity sections, we calculate Eulerian mean transect across the shelf break (Figure 2) in the along-shelf direction (southwest) and the cross-shelf direction (southeast). The Eulerian mean Shelfbreak Jet is centered over the 115-m isobath (161 km from Ambrose Light), has a maximum along-shelf velocity of 0.11 m s^{-1}, an e-folding width of 50 km, and an e-folding depth of 90 m. The maximum velocity occurs in the surface bin, which is centered at 18-m depth, and velocities decrease with depth. These time-averaged jet properties are similar with previous work based on ADCPs, hydrographic data, and moorings, though our maximum jet velocity is on the lower bound of velocities previously reported (e.g., Flagg et al., 2006; Fratantoni & Pickart, 2007; Linder & Gawarkiewicz, 1998). The transport calculated by integrating the along-shelf velocity within the e-folding isotach (0.04 m s^{-1}) is 0.16 Sv, where the transport includes only the directly measured velocity.

This mean transport is smaller than most previous work (Table 1); however, this is largely because shipboard ADCPs are not able to measure the surface layers where the strongest Shelfbreak Jet velocities are typically found. In order to obtain a better estimate of the mean Shelfbreak Jet transport, we extrapolate data to the surface. At each horizontal bin within the Shelfbreak Jet, we choose either a linear or exponential fit depending on the vertical structure of the existing data in the deeper bins. Each fit is then used to calculate estimates for the along-shelf velocities at the surface (shaded contours above the dashed line in Figure 3). The estimated mean maximum jet velocity is 0.12 m s^{-1}, with the same e-folding length and depth scales of 50 km and 90 m, respectively. Using these estimates of velocities in the shallowest layers gives transport within the mean Shelfbreak Jet of 0.21 ± .02 Sv, which is similar to previously reported values (Table 1). Our error estimate is calculated from resampling the 1,362 transects with replacement and calculating a new mean Shelfbreak Jet using the randomly selected resampled transects. We iterate this resampling 1,000 times, calculating the Eulerian mean transport of the Shelfbreak Jet in each iteration, and 95% of the resampled

Table 1
Calculations of the Shelfbreak Jet Transport

Measurement	Transport (Sv)	Location	Year	Season	Coordinate	Citation
ADCP	0.21 ± .02	New Jersey	1994–2018	Annual	Eulerian	
ADCP	0.37 ± .04	New Jersey	1994–2018	Annual	Stream Coordinates	
ADCP	0.4	New Jersey	1994–2002	Annual	Eulerian	Flagg et al. (2006)
Hydrography	0.16	New Jersey	1900–1990	Annual	Eulerian	Linder and Gawarkiewicz (1998)
Hydrography	0.24	Nantucket Shoals	1900–1990	Annual	Eulerian	Linder and Gawarkiewicz (1998)
Hydrography	0.25	MAB	1990–2001	Apr–Sep	Eulerian	Fratantoni and Pickart (2007)
ADCP	0.46 ± .32	Nantucket Shoals	1995–1997	Fall–Winter	Stream Coordinates	Fratantoni et al. (2001)

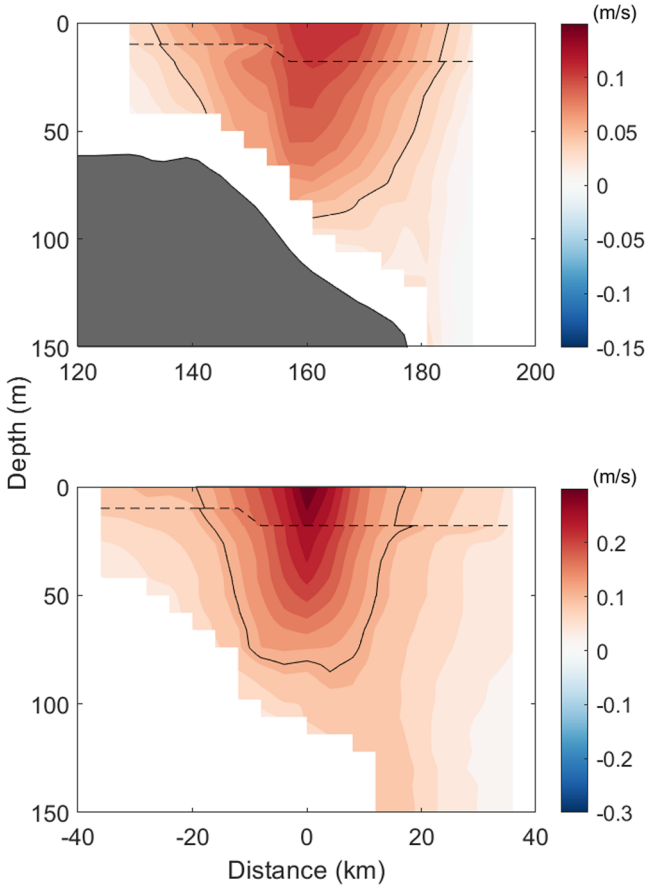

Figure 3. Eulerian mean along-shelf velocity (top) and stream coordinates mean along-shelf velocity (bottom) with extrapolated data above the dashed line. The e-folding isotach (black line) is plotted for each case.

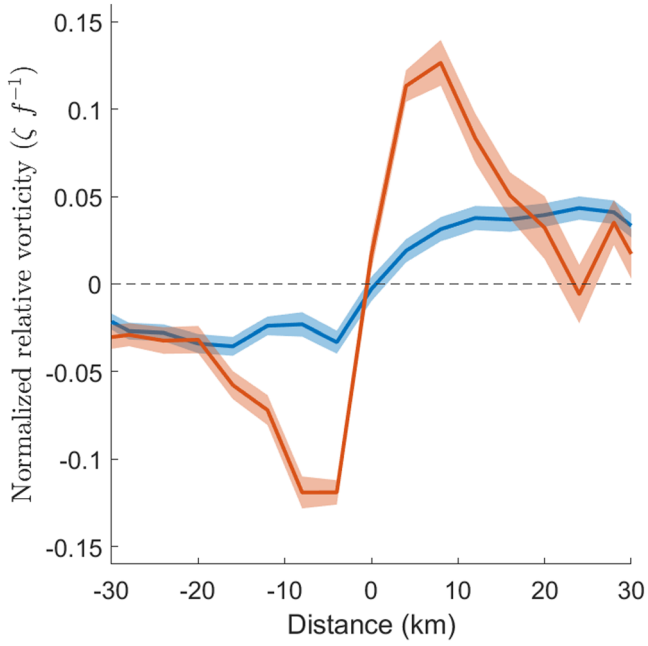

Figure 4. Eulerian mean (blue) and stream coordinates mean (red) normalized relative vorticity from the shallowest bin of velocity data. Mean standard errors of the normalized relative vorticity are shown in the shaded colors.

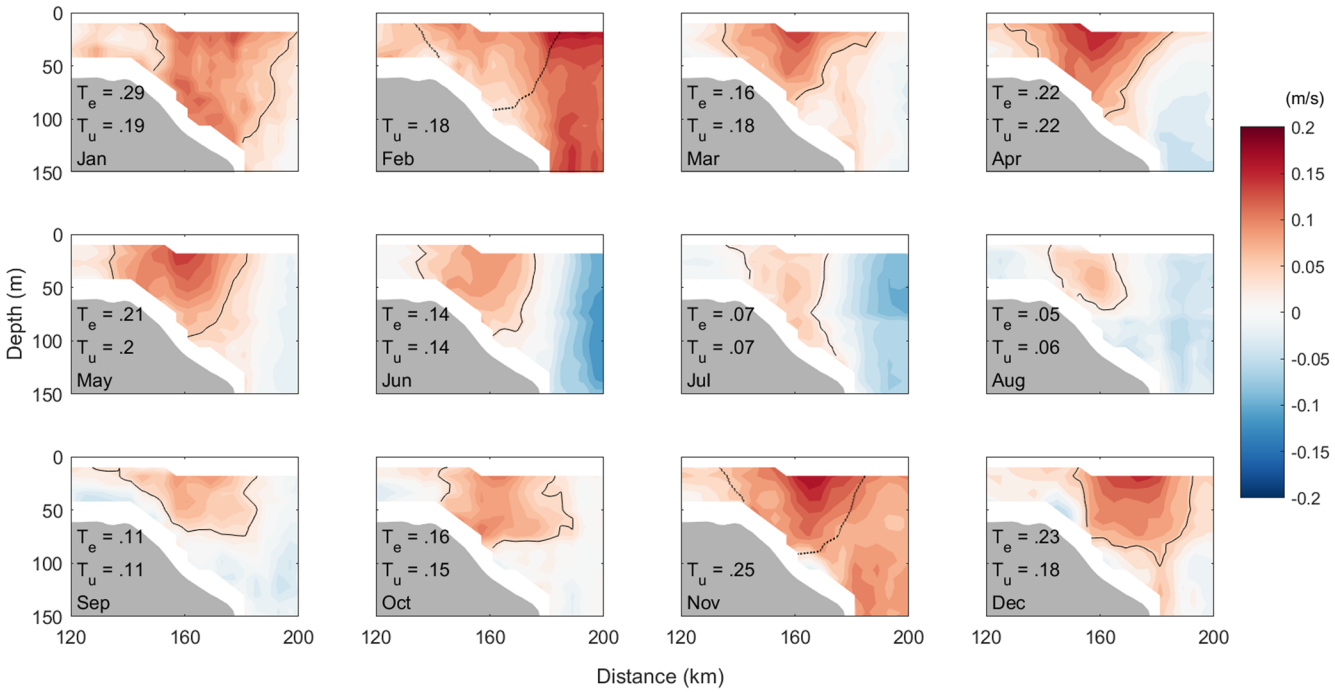

Figure 5. Eulerian mean along-shelf velocities in each month. T_e is the transport in Sverdrups within each months e-folding isotach (solid black line) calculated based on the maximum velocity in each month. T_e cannot be calculated during February and November. T_u is the transport in Sverdrups within the climatogical e-folding isotach (dashed black line in February and November) shown in Figure 2.

Eulerian mean transports fall within the aforementioned error range. These estimates suggest that about 24% of the mean Shelfbreak Jet transport is carried in the upper 14 m of the water column.

We calculate the absolute value of the normalized relative vorticity, or Rossby number, here defined as $|\frac{\partial u}{\partial y} \cdot f^{-1}|$, for the Eulerian mean Shelfbreak Jet in the shallowest layer of data (bin centered at 18 m; Figure 4). We do not calculate the normalized relative vorticity for the surface layer since we do not have direct observations of the surface velocities. The relative vorticity on either side of the Shelfbreak Jet is not strongly peaked. The ratio of cyclonic to anticyclonic relative vorticity within the e-folding width scale of 50 km is 1.17. The normalized relative vorticity reaches a maximum value of 0.05, reinforcing that geostrophy is a good approximation in this region.

Capitalizing on the large number of transects measured by the Oleander over the years, we are able to create a monthly climatology over the shelf break in contrast to past climatologies that have been limited to bimonthly or seasonally averaged analyses. The along-shelf velocities in this climatology show a strong variability both in the core of the Shelfbreak Jet and over the slope (Figure 5). The core of the climatological Shelfbreak Jet reaches a maximum in April–May and a secondary maximum in November. During these peak months, the Shelfbreak Jet has surface-intensified maximum velocities around 0.16 m s^{-1} and closely resembles the velocity structure of the overall Eulerian mean section. Summer months have the weakest maximum Shelfbreak Jet velocity, with maximum velocities only reaching 0.07 m s^{-1} in July and August. The summer also differs from the rest of the year, in that the Shelfbreak Jet has a subsurface velocity maximum. In July, the maximum velocity occurs in the depth bin centered at 58 m, and in August the maximum velocity is found in the depth bin centered at 42 m.

The transport calculations from this monthly climatology show a seasonal cycle similar to that of velocity. Here we calculate transport in two different ways though we note that each methodology likely underestimates the total transport as we do not extrapolate data to the surface here. In the first, T_e is calculated by finding the e-folding isotach in each month and then calculating the transport within that cross-sectional area. In the second, T_u relies on the area within the e-folding isotach from the mean Eulerian Shelfbreak Jet to calculate the transport. Both of these methods for calculating the transport are very similar except in January, where the area used to calculate the transport for T_e is 50% larger than the area for T_u. With both methodologies, the highest transport occurs in December and January, with a secondary peak in April and

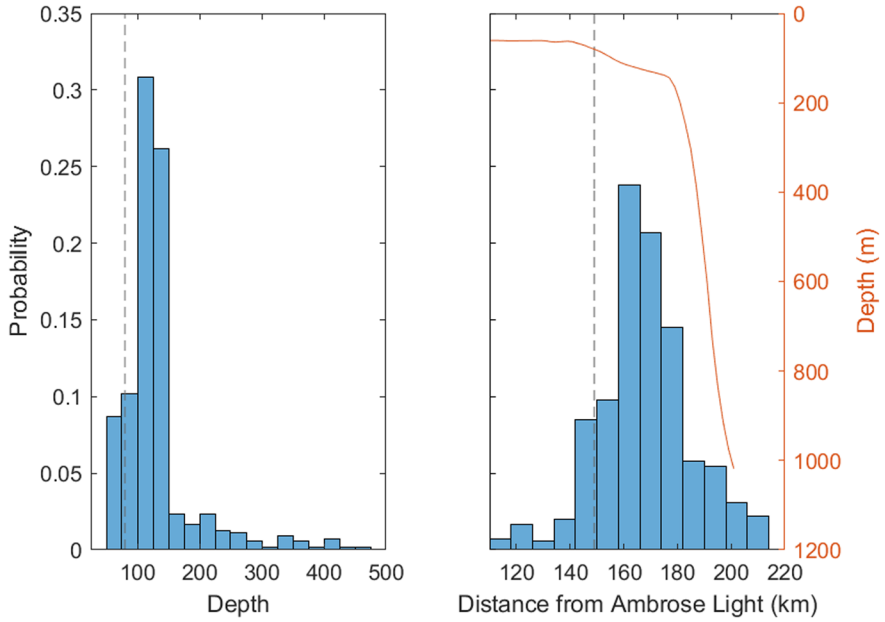

Figure 6. Normalized probabilities of the location of the Shelfbreak Jet in isobath (left) and distance from Ambrose Lighthouse (right). The mean grounding position of the Shelfbreak Front (80-m isobath) is found at 149 km and plotted in the dashed gray line (Linder & Gawarkiewicz, 1998).

May. In summer, the jet has the smallest maximum jet velocities and also the smallest cross-sectional area, which both contribute to the weakest transport. The transport in summer is approximately 1/4 that of the transport in December/January.

3.2. Stream Coordinate Mean Shelfbreak Jet Velocity Structure and Transport

The Eulerian framework is useful for studying the overall velocity structure over the shelf break; however, the Shelfbreak Front and Jet are known to have meander amplitudes up to 15 km in the cross-shelf direction (Gawarkiewicz et al., 2004). In order to study the properties of the meandering Shelfbreak Jet, it is helpful to use a stream coordinates framework (Flagg et al., 2006; Fratantoni et al., 2001). Using our methodology to identify the Shelfbreak Jet (section 2.1.3), we find a jet in 44% of the ADCP transects. For the remaining 56% of the sections, a jet cannot be identified because of poor data quality and/or because the jet is absent. When only considering transects that have "good" data over the shelf break, defined here as sections with over 70% data return, the Shelfbreak Jet is identified in 61% of the total 669 sections. This shows that the Shelfbreak Jet is intermittent in space and time on the New Jersey Bight. The remaining discussion is based on only sections with over 70% data return.

Although the Shelfbreak Jet is present in 61% of the (good) transects, there is large monthly variability in this percentage. The Shelfbreak Jet is most consistently identified during April (74% of the good sections), and least consistently identified in August (39% of the good sections). On a seasonal timescale, the jet is more common in spring and fall and less commonly found in summer and winter. This seasonal cycle is consistent with our Eulerian climatology in which the fastest Shelfbreak Jet core velocities and highest transports were found in spring and fall.

We identify the Shelfbreak Jet most often in the same cross-shelf position as the core of the Eulerian mean Shelfbreak Jet, over the 115-m isobath, 162 km from Ambrose Light (Figure 6). The jet core meanders within ±20 km of its mean position around 80% of the time, relatively consistent with the 50-km length scale of the Eulerian mean Shelfbreak Jet. This meander amplitude keeps the Shelfbreak Jet concentrated over the 70- to the 150-m isobaths. Occasionally, we observe displacements of the core up to 20 km away from the mean position, similar to previous reports of large amplitude Shelfbreak Jet meanders (Gawarkiewicz et al., 2004). The Shelfbreak Jet is strongly trapped by bathymetry. The jet is found onshore of the 150-m isobath over 75% of the time, which is the isobath where the slope is the steepest on this transect. Onshore jet displacements reach the 60-m isobath, while rare offshore displacements extend past the shelf break to depths over 1,000 m.

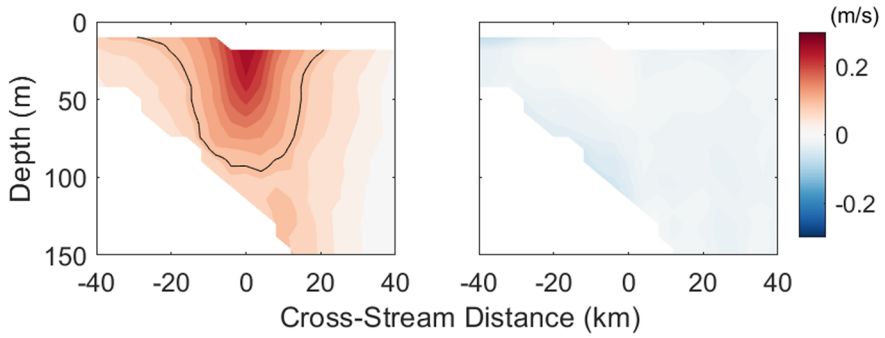

Figure 7. Stream coordinates mean along-stream velocity (left column) and cross-stream velocity (right column) of the Shelfbreak Jet. The e-folding isotach (black line) is plotted for the mean along-stream velocity. The Shelfbreak Jet is identified in 546 sections.

Because the Shelfbreak Jet is intermittent and also meanders in the cross-shelf direction, a stream coordinate framework is useful to study the properties of the jet. We create a mean stream coordinate Shelfbreak Jet by taking every good section in which the jet is identified, and rotating the velocity in each section into the along-stream direction, which is the direction of the maximum Shelfbreak Jet velocity, and the cross-stream direction. We align and project each transect in horizontal space, accounting for the differences in cross-stream distance due to the projection, where the maximum Shelfbreak Jet velocity is at the origin of the distance axis, and keep the depth coordinates the same.

The stream coordinate mean Shelfbreak Jet has a surface-intensified velocity maximum of 0.27 m s^{-1} and has an e-folding width scale of 40 km and depth scale of around 80 m (Figure 7). Transport within the stream coordinate mean Shelfbreak Jet is 0.34 Sv without extrapolating data to the surface. Repeating the same fit and extrapolation techniques with the stream coordinates mean as described earlier for the Eulerian mean gives a maximum velocity of 0.32 m s^{-1}, a length scale of 35 km, and a depth scale of 85 m (Figure 3). Including extrapolated velocities near the surface increases the transport estimate to 0.37 ± .04 Sv, which is a similar increase in magnitude to that of the Eulerian mean case, but represents only a 12% relative increase. The stream coordinates jet has a smaller length scale when including the surface velocities, and thus, the transport does not increase as much in a relative sense.

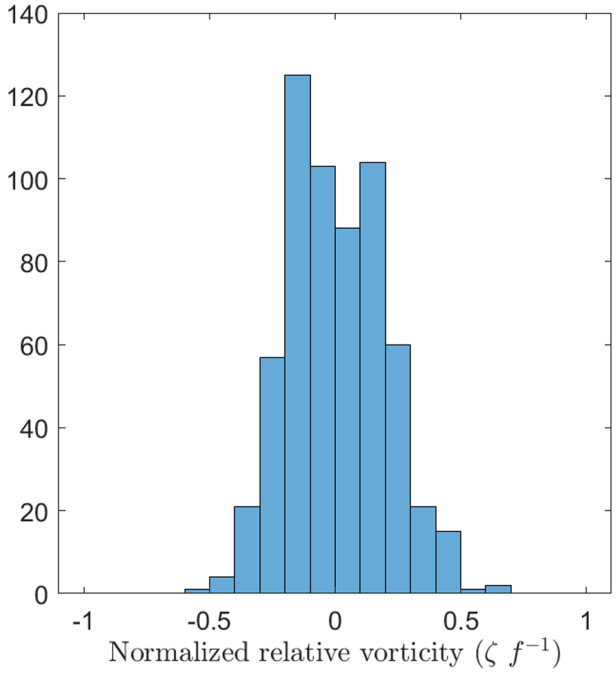

Figure 8. Histogram of the maximum and minimum normalized relative vorticity, across the Shelfbreak Jet in every transect when the jet is identified.

The normalized relative vorticity in the shallowest directly measured layer (bin centered at 18 m) of the stream coordinate mean velocity section is distinctly more peaked than that of the Eulerian mean section (Figure 4). The maximum normalized relative vorticity in the stream coordinate mean section reaches 0.15, which is larger than the maximum reached in the Eulerian mean section. In the stream coordinate framework, the ratio of cyclonic to anticyclonic relative vorticity is smaller than the Eulerian ratio at 1.02. However, if we calculate this ratio for each transect in which the Shelfbreak Jet is identified, the median cyclonic to anticyclonic ratio is 1.12.

For both the stream coordinate mean and the Eulerian mean, our calculated ratio of cyclonic to anticyclonic relative vorticity differs from the expected 2:1 ratio that was found by Nantucket Shoals (Linder & Gawarkiewicz, 1998). This could be due to differences in location or methodologies as Linder and Gawarkiewicz (1998) calculated velocities from thermal-wind balance, included velocities up to 5-m depth whereas our shallowest bin is centered at 18 m depth, and looked at bimonthly averages and not the mean. However, we still see the stronger shear on the slope side of the Shelfbreak Jet, consistent with studies from Nantucket Shoals to just north of Cape Hatteras (Fratantoni et al., 2001; Gawarkiewicz et al., 1996). We create a histogram of the maximum anticyclonic and cyclonic relative vorticity values in the Shelfbreak Jet in every

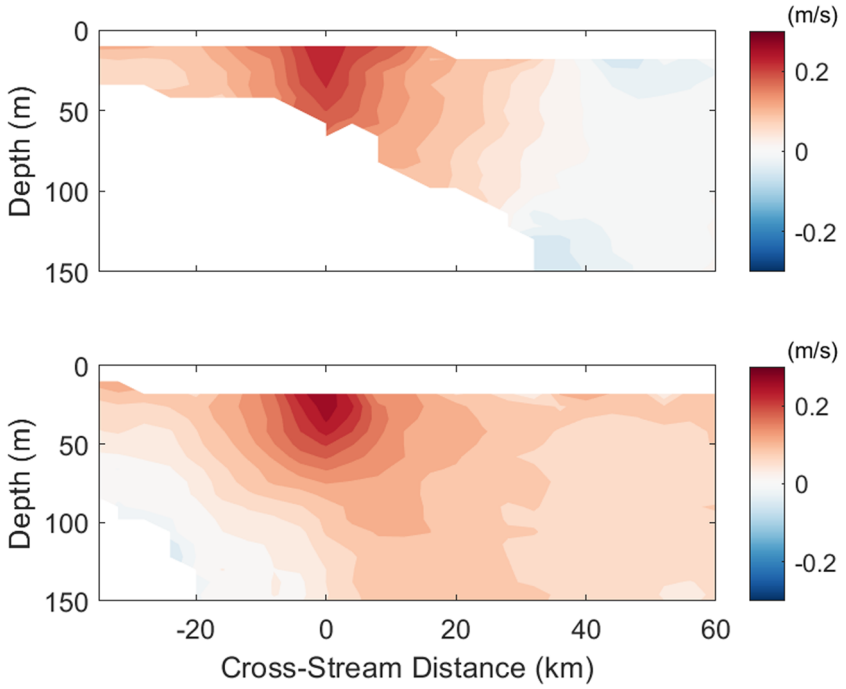

Figure 9. Stream coordinate along-stream velocity means (in m s^{-1}) when the Shelfbreak Jet is identified onshore of its mean position (top, calculated from 105 transects) and offshore of its mean position (bottom, calculated from 71 transects).

transect where we identify the jet (Figure 8). We do not take the absolute value of the normalized relative vorticity here to differentiate between the values of anticyclonic and cyclonic. The relative vorticity stays below a magnitude of 0.5, on both sides of the jet, 94% of the time.

The monthly climatology of the velocity sections calculated in stream coordinates is similar to the climatology calculated in an Eulerian framework, with the strongest velocities from November through April and the weakest velocities in June through August. One striking difference between the stream coordinate versus Eulerian mean climatologies is that the structure of the jet in the stream coordinates case remains consistent throughout the year, resembling the velocity structure of the stream coordinates mean (Figure 7). We identify the jet most consistently in Spring and Fall.

4. Conditional Averageing for a Broader View

4.1. Variability in the Position of the Jet

In order to study the variability in the position of the Shelfbreak Jet, we create stream coordinate means conditionally averaged when the Shelfbreak Jet is displaced over 10 km from the mean position, in both the onshore and offshore direction (Figure 9). Overall, we find shifts in the position of the Shelfbreak Jet are accompanied by changes in the along-shelf velocity structure. The mean jet when shifted offshore has a maximum velocity of 0.30 m s^{-1}, which is larger than the 0.24 m s^{-1} maximum velocity of the mean jet when shifted onshore. During time periods when the Shelfbreak Jet is shifted onshore, there is a reversal of the stream coordinate velocity over the slope, which is not seen during time periods when the Shelfbreak Jet is offshore of its mean position.

The vertical structure of the Shelfbreak Jet also varies in concert with the onshore/offshore position of the jet. We calculate the velocity shear for the stream coordinate overall mean Shelfbreak Jet (not shown), as well as for both the onshore and offshore shifted Shelfbreak Jet (Figure 10). In the (overall) stream coordinate mean Shelfbreak Jet velocity section, the velocity shear decreases in the core of the jet from surface to bottom. The variability and scatter of this velocity shear also decrease with depth. The conditional averages show that when the Shelfbreak Jet is found further offshore, the velocity shear also decreases with depth. However, when the jet is onshore of its mean position, the along-shelf velocity decreases more linearly with depth.

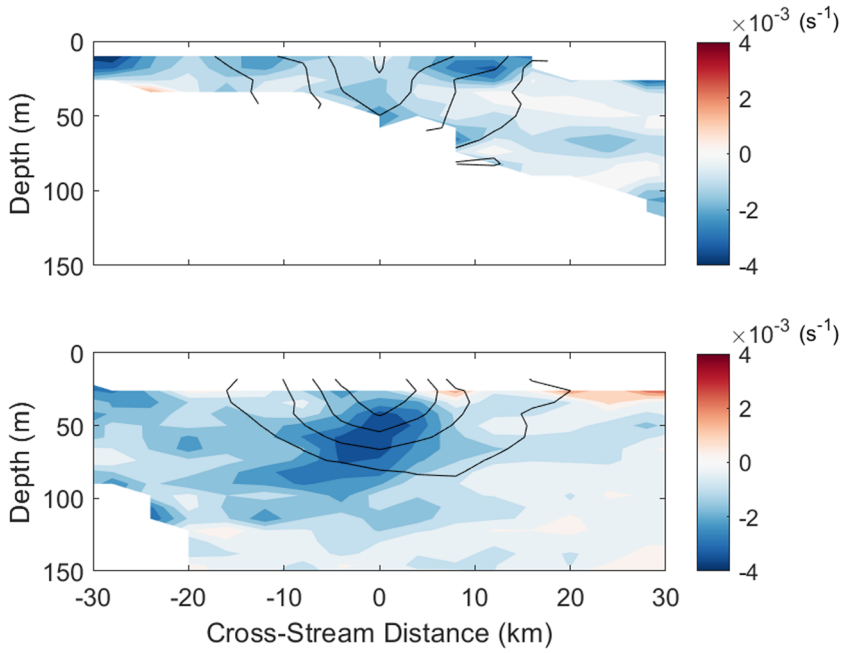

Figure 10. Stream coordinate along-stream velocity shear ($\partial u/\partial z$ s^{-1}) in the colored contours when the Shelfbreak Jet is identified onshore of its mean position (top) and offshore of its mean position (bottom). Solid black contours are the stream coordinate along-stream velocity means for the onshore and offshore shifted Shelfbreak Jet from Figure 9.

The velocity shear is also an order of magnitude larger during time periods when the jet is offshore relative to onshore. Typically, half of the Shelfbreak Jet's transport is baroclinic; however, here the jet is a lot less baroclinic when it is shifted onshore (Fratantoni & Pickart, 2007). This could mean that the onshore shifted Shelfbreak Jet is consistent with a weaker Shelfbreak Front or that the Jet when found further onshore is not associated with the Shelfbreak Front.

To provide spatial context for the conditionally averaged mean velocity sections for an onshore-shifted and offshore-shifted Shelfbreak Jet, we create corresponding composite maps from satellite SST and SSH data when the jet is found onshore and offshore of its mean position (Figure 11). When the jet is identified offshore, small negative SSH and SST anomalies are found along the Oleander track. During time periods when the Shelfbreak Jet is shifted onshore, there are large positive SST and SSH anomalies north of the mean position of the Gulf Stream. These SST anomalies extend from the Gulf Stream, through the Slope Sea, and onto the outer shelf, while the SSH anomalies only extend into the Slope Sea. These maps suggest that the position of the Shelfbreak Jet is related to the SSH and SST of the Gulf Stream just east of Cape Hatteras.

The relationship between variability of the Gulf Stream position and the variability of the Shelfbreak Jet has not been well established. Past research showed that the Gulf Stream was not the main driver of the Shelfbreak Jet variability south of New England, northeast of the Oleander Line (Fratantoni & Pickart, 2003), while other studies have found significant correlations between the two currents at study sites further downstream of the New England Shelfbreak Jet (Bane et al., 1988; Rossby & Benway, 2000). Bane et al. (1988) found a positive correlation between the proximity of the Gulf Stream to the shelf and Shelfbreak Jet velocities just north of Cape Hatteras. They hypothesized that when the Gulf Stream was closer to the shelf, it constricts the Slope Sea gyre, which leads to enhanced Shelfbreak flows toward Cape Hatteras. Rossby and Benway (2000) also found evidence of connections between shelf flows and the position of the Gulf Stream, with the position of the Gulf Stream highly correlated with the Gulf Stream's surface salinity. They suggested that the surface salinity of the Gulf Stream is controlled by the equatorward freshwater transport in the Slope Sea. Reduced transport on the shelf and in the Slope Sea leads to a weaker freshwater anomaly, which is correlated with a more northward position of the Gulf Stream. The correlation between the Slope Sea and Gulf Stream position was further shown by Peña-Molino and Joyce (2008), where they found a correlation between temperatures in the Slope Sea and the Gulf Stream position, also suggesting an advective mechanism for the Slope Water influencing the Gulf Stream position.

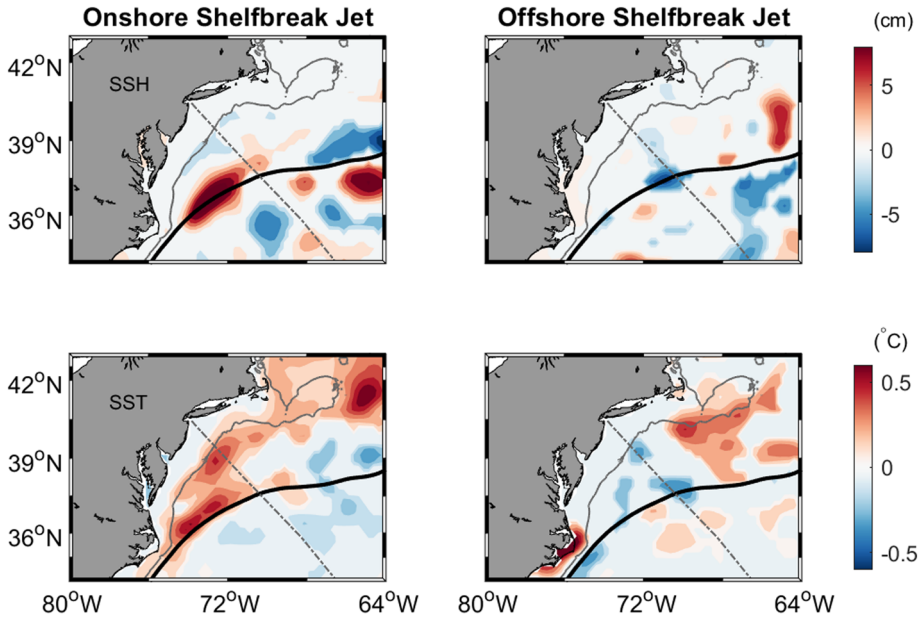

Figure 11. Composite maps of SSH anomalies (cm, top row) and SST anomalies (°C, bottom row) when the Shelfbreak Jet is identified onshore of its mean position (left column) and offshore of its mean position (right column). Colored contours are not shown if the mean standard errors overlap with zero. The gray dashed line is the Oleander path, the gray solid line is the 80-m isobath, and the solid black line is the mean position of the 25-cm SSH contour, which is a proxy for position of the Gulf Stream.

Our composite maps are consistent with the correlations found in Rossby and Benway (2000), as our onshore-shifted Shelfbreak Jet has reduced along-stream velocities simultaneous with a northward-shifted Gulf Stream as seen by the positive SSH anomaly around the mean position of the Gulf Stream axis (Figure 11). This relationship is affirmed by calculating the correlation of the latitude of the 25-cm SSH contour just east of Cape Hatteras (72–74°W), a proxy for the Gulf Stream position (Andres, 2016), and the position of the Shelfbreak Jet gives a significant correlation at the 95% confidence level. In addition, the mean latitude of the 25-cm SSH contour just east of Cape Hatteras (72–74°W) is found on average $\left(\frac{1}{8}\right)°$ further north in time periods where the jet is shifted onshore. This suggests a different mechanism than the Slope Sea gyre constriction suggested by Bane et al. (1988) whereby the Gulf Stream was posited to impact the Shelfbreak Jet. Off of New Jersey, there is a simultaneous shift of the Gulf Stream and Shelfbreak Jet position. Our results do not contradict the findings of Fratantoni and Pickart (2003), as their dominant mode of Shelfbreak Jet variability was at a 13-day period, a timescale that we cannot consistently resolve with the Oleander ADCP data, which are collected weekly at best. Taken as a whole, the studies suggest that different processes are likely operating at different timescales leading to a complicated relationship between the Shelfbreak Jet and the Gulf Stream.

4.2. Determining the Factors Causing Jet Presence or Absence

As previously discussed, the Shelfbreak Jet is only present in 61% of the ADCP velocity sections. To better establish what is driving the variability of the Shelfbreak Jet, we examine what causes the complete shutdown of the Shelfbreak Jet southeast of New Jersey. We calculate Eulerian mean transects from the sections in which a Shelfbreak Jet is identified, and from the sections in which it is not identified (Figure 12). With this conditional averaging, the Eulerian mean from transects with the Shelfbreak Jet identified resembles the velocity structure of the total Eulerian mean (Figure 2), but with a stronger velocity core reaching 0.15 m s^{-1}. As expected, when the Shelfbreak Jet is not identified, the magnitude of the Eulerian mean along-shelf velocities are weak with velocities around 0.04 m s^{-1}. In contrast, cross-shelf velocities on the shelf are stronger when the Shelfbreak Jet is not present, reaching up to 0.1 m s^{-1} in the onshore direction.

Over the continental slope, the differences in the mean along-shelf velocities for the conditional averages with and without a Shelfbreak Jet are even more striking. There are southwest velocities over the slope in both cases, resembling the Slope Jet previously documented from Oleander data (Flagg et al., 2006); however,

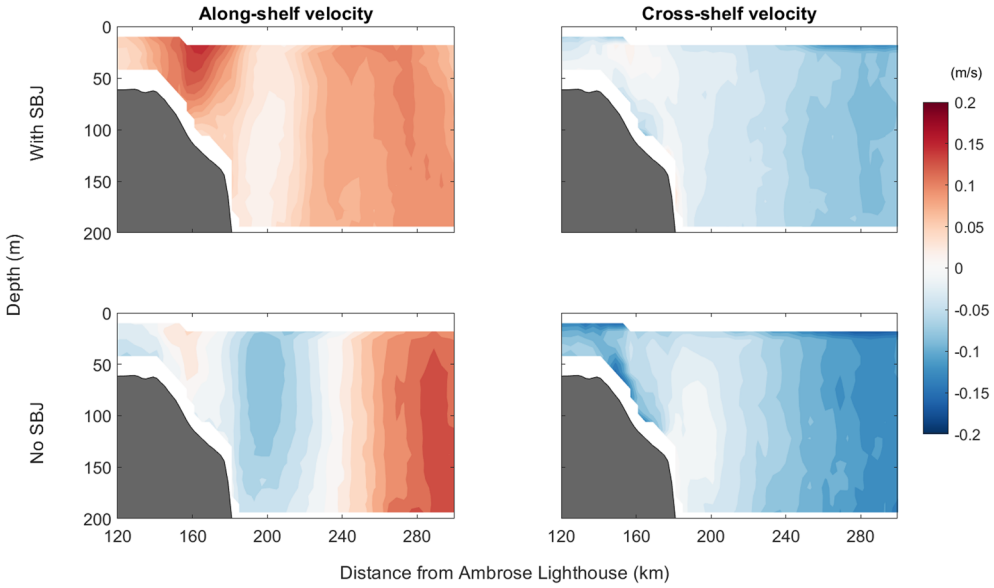

Figure 12. Eulerian mean along-shelf velocity (left column) and cross-shelf velocity (right column) during time periods when the Shelfbreak Jet is identified (top row) and time periods when the Shelfbreak Jet is not present (bottom row).

only in the mean velocity section generated from the transects with no Shelfbreak Jet do we see northeastward velocities adjacent to the shelf. These northeastward velocities abutting the shelf and adjacent to a Slope Jet suggest an anticyclonic circulation, which is the signature of a Warm Core Ring in the Slope Sea. This strongly suggests that Warm Core Rings can serve to disrupt the Shelfbreak Jet.

To examine this further, we construct composite maps showing SSH and SST anomaly fields 1 month before, during, and 1 month after we cannot identify the Shelfbreak Jet in an individual ADCP section (Figure 13). The composite SSH anomalies show a positive anomaly tracking from northeast of the Oleander line in the Slope Sea, to south of the Oleander line afterward. This positive SSH anomaly resembles the signature of a Warm Core Ring on the slope, consistent with the along-shelf velocity signals observed in the conditionally averaged ADCP sections. Using SSH eddy tracking (Chelton et al., 2011), when the Shelfbreak Jet cannot be identified, anticyclonic eddies are observed more frequently on the Oleander track in the Slope Sea as compared to time periods when the Shelfbreak Jet is identified. Furthermore, the average azimuthal velocity of those eddies observed when the Shelfbreak Jet is not identified is almost twice that of the average azimuthal velocity of eddies observed during time periods when the Shelfbreak Jet is observed. Research is ongoing to study the impact of these individual tracked rings on the Shelfbreak Jet and shelfbreak region.

During time periods without the Shelfbreak Jet, there is also a broad negative SSH anomaly over the shelf, leading to a reduced SSH gradient across the shelf break. The amplitude of this reduced SSH gradient supports a 0.04 m s^{-1} reduction in SSH-derived geostrophic velocity relative to the total mean SSH-derived geostrophic velocities across the shelf break. The total in situ velocity difference at the shelf break between time periods without the jet and the total Eulerian mean velocity is 0.09 m s^{-1}, suggesting that the change in SSH gradients only account for half of this observed difference. Here we find disruptions in the Shelfbreak Jet may also be in large part due to ageostrophic forces. Ageostrophic velocities have been calculated to make up significant contributions to Shelfbreak Jet meanders (Gawarkiewicz et al., 2004). We note that a simple linear superposition of an anticyclonic ring and a jet may also reverse the flow of the jet depending on the relative strength of both (Gawarkiewicz et al., 2001).

In addition to the positive SSH anomalies associated with times when there is no Shelfbreak Jet at the Oleander Line, we also see strong positive SST anomalies during these same time periods. The composite SST map shows a positive SST anomaly from Nantucket Shoals, through the entirety of the MAB 1 month before and during time periods without the Shelfbreak Jet. This anomaly signal then advects further south 1 month later. The warm anomalies over the slope are collocated with the SSH anomalies in the slope, which is consistent for a Warm Core Ring in the Slope Sea. Additionally, these positive SST anomalies are continuous from the Slope Sea into the Shelf, suggesting that there is a cross-shelf exchange process that drives the

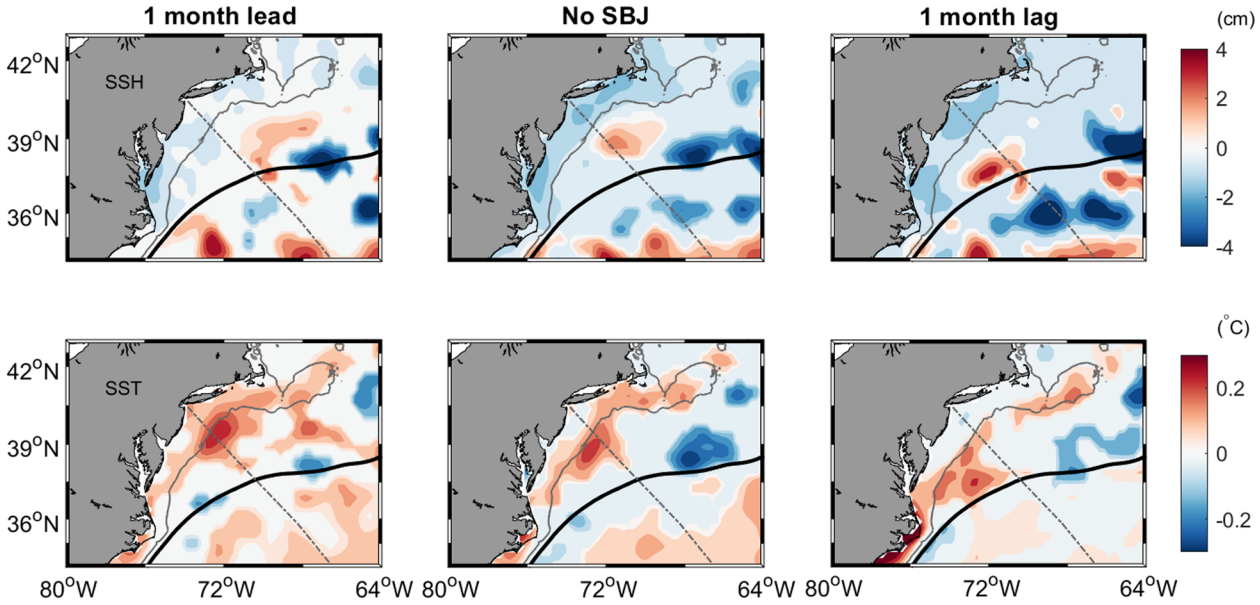

Figure 13. Composite maps of SSH anomalies (cm, top row) and SST anomalies (°C, bottom row) around the times that the Shelfbreak Jet cannot be identified in the ADCP data. Composites are shown 1 month before (left column), concurrently with (middle column), and 1 month after (right column) the Shelfbreak Jet is not identified in ADCP sections with over 70% data return. Contours not shown if the mean standard errors overlap with zero. The gray dashed line is the Oleander path, the gray solid line is the 80-m isobath, and the solid black line is the mean position of the 25-cm SSH contour, which is a proxy for the position of the Gulf Stream. Note the color bar ranges are both halved from Figure 11.

warmer slope water onto the shelf. This is consistent with the conditionally averaged ADCP sections discussed above, which show that for times when the Shelfbreak Jet is absent, the (Eulerian) mean cross-shelf (onshore) flow is enhanced. During these same time periods without the Shelfbreak Jet, the ADCP measurements showed enhanced onshelf flow, which would allow for the Warm Core Ring water to advect onto the shelf.

4.3. Interannual Variability and Connections with Temperature

Considering the warm SST anomalies concurrent with time periods without the Shelfbreak Jet, we would expect the velocities over the shelf break to be related to the shelf temperature. In order to study this relationship, we utilize the velocity and temperature profile measurements from the Oleander. We create two velocity time series, one using the Eulerian framework and one using the stream coordinate framework. These time series are created by spatially averaging the top 50 m in each velocity transect in a 20-km region with the region differing in the two frameworks. In the Eulerian framework, we spatially average each transect's velocities in a region centered at the Eulerian mean location of the Shelfbreak Jet core (115-m isobath) and then define this time series as the velocity at the shelf break. For the stream coordinates framework, we only use the sections where we have identified the jet and spatially average the velocity data in a 20-km region centered at the location of the identified Shelfbreak Jet. We define this stream coordinate framework as the time series of Shelfbreak Jet velocity. Lastly, we use a 12-month moving average for both to deseason and temporally grid the sections.

Both the time series of the velocity over the shelf break and the Shelfbreak Jet velocity demonstrate large interannual variability (Figure 14). The mean velocities at the shelf break are 0.07 m s^{-1} with a standard deviation of 0.035 m s^{-1}. Minimum values of the velocity over the shelf break time series are below zero, indicating poleward flow, while peak velocities reach 0.14 m s^{-1}. Large changes due to persistent Warm Core Rings appear in the time series at the end of 2001 and during 2008, exhibited by the near zero velocity. The time series of Shelfbreak Jet velocity exhibits a mean of 0.19 m s^{-1}, which is much higher than the mean velocity at the shelf break. However, the standard deviation of the Shelfbreak Jet velocity time series was lower at 0.025 m s^{-1}. During the time periods when ring influences can be seen in velocity at the shelfbreak, we do not see anomalous deviations of the Shelfbreak Jet velocity time series as they are filtered out in the identification method.

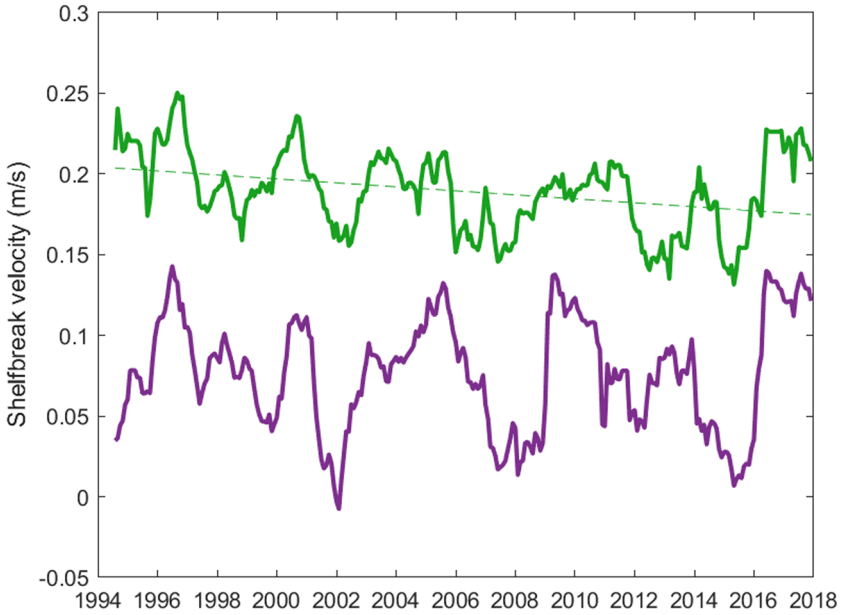

Figure 14. Time series of the velocity over the shelf break (purple) and Shelfbreak Jet velocity (green), as defined in section 4.3. Both time series are 12-month moving averaged. The dashed lines show the long term trends. Only the linear trend of the Shelfbreak Jet velocity is significantly different from zero.

The methodology for defining the time series of shelf temperatures was previously described in Forsyth et al. (2015). This temperature time series only uses observations on the shelf, defined as onshore of the 80-m isobath. In this study, we use a 12-month moving average on the monthly shelf temperatures instead of an annually averaged value. Here we compare the time series of velocity at the shelf break with shelf temperature. These two time series are maximally and significantly correlated at a 2-month lag, with velocity leading temperature ($r^2 = 0.29$, $p < 0.05$; Figure 15). This correlation is significant at the 95% confidence level accounting for effective degrees of freedom due to autocorrelation, from a 1- to a 3-month lag, and is significant at the 90% level from a 1-month lead to a 5-month lag.

Enhanced along-shelf velocities lead cold time periods on the shelf, while decreased along-shelf velocities precede warmer time periods on the shelf. The difference in shelfbreak velocities in cold and warm periods

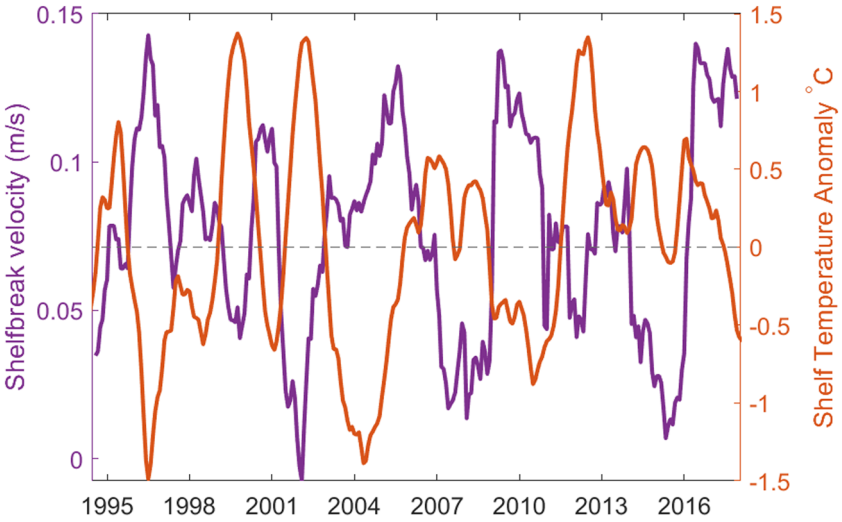

Figure 15. Time series of the velocity over the shelfbreak (purple) and temperautre on the shelf (red). Both time series are deseasoned with a 12-month moving average. The two time series are significantly anticorrelated ($p < 0.05$) with a 1- to 3-month lag, with velocity leading temperature.

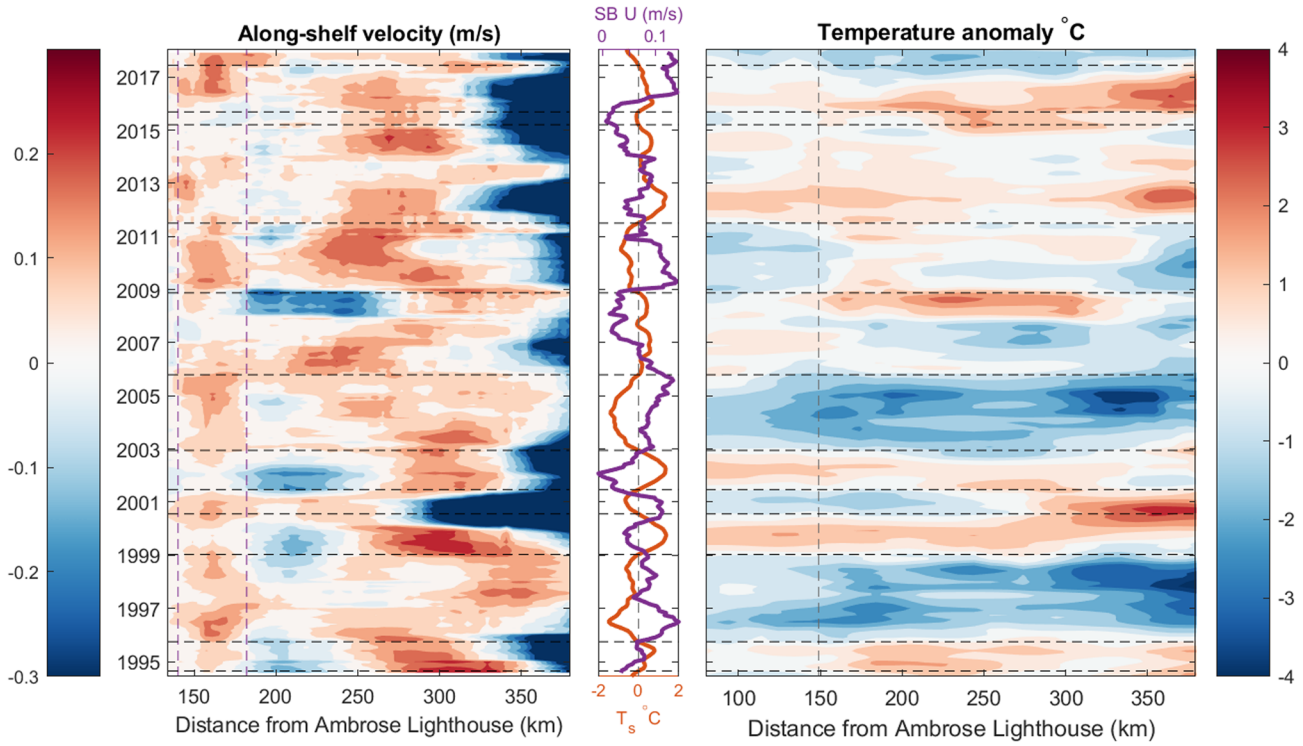

Figure 16. Hovmuller diagram of the upper 50-m along-shelf velocity (left contour plot) and upper 50-m temperautre (right contour plot). The middle panel shows a time series of the mean shelfbreak velocities from 140–182 m (purple dashed lines in left panel) and upper 50 m in purple and the mean shelf temperatures onshore of the 80-m isobath in red (vertical gray dashed line in left and right contour plots).

is on average 0.03 m s^{-1}. Stronger along-shelf flows would enhance the transport of cooler waters from upstream. Warm Core Rings are another possible reason for the correlation between Shelfbreak Jet velocities and temperature. A Warm Core Ring impinging on the shelf can both increase the temperature on the shelf and reduce/reverse the Shelfbreak Jet velocities. As discussed previously, when the jet is not identified, there is enhanced onshore flow. A warmer shelf is consistent with enhanced slope water transport onto the shelf, especially if ring water remains in the Slope Sea.

This connection between temperature and velocity is made more clear looking across the entire shelf and slope. Here we show the Eulerian surface (top 50-m) along-shelf velocities and temperatures, using the same methodology as the time series above, with the exception that we do not spatially average these data (Figure 16). Cross-shelf velocities are not shown, as the variability is small relative to the along-shelf velocity variability. During periods of time with cold anomalies on the shelf, the Shelfbreak Jet is clear, while during warmer time periods the Shelfbreak Jet is not as clearly seen. This is consistent with our Shelfbreak Jet identification, where during cold periods, the Shelfbreak Jet is identified 68% of the time, and only identified 57% of the time when the shelf is warm. The continuous Shelfbreak Jet in cold time periods is also consistent with an advective mechanism driving along-shelf advection of cooler waters. Stronger and more consistent transport of cooler upstream waters to the MAB shelf could reduce the temperature on the shelf.

Warm time periods are often associated with an anticyclonic velocity signature over the slope, with north-east velocities adjacent to the shelfbreak. When rings are observed in the along-shelf velocity, we can see a concurrent warm anomaly in temperature over the slope and shelf. During four of the six warm periods identified, (1995, 1999–2000, 2002, and 2008), we can see Warm Core Rings abutting the shelf for at least some portion of time, with three of these time periods beginning with Warm Core Rings over the shelf. Of the two remaining warm periods identified without Warm Core Rings, the warming beginning in late 2011 has been documented and discussed as primarily being caused by atmospheric forcings (Chen et al., 2014). While many of the warm time periods can be attributed to oceanic and atmospheric processes, the variability driving cooling time periods has not been the focus of much research and remains an open question.

4.4. Long-Term Shelfbreak Jet Variability

There is no significant long-term trend in the time series of the velocity at the shelf break. In contrast, the Shelfbreak Jet velocity time series has decreased in velocity over the 25 years of data (Figure 14). We estimate a statistically significant reduction in velocity of 0.03 m s^{-1} over the entirety of the data set. This may be related to a reduction in density gradients across the front. Using the XBT data from the Oleander between 1992 and 2018, we calculated the average trend in temperature on either side of the mean position of the Shelfbreak Jet. The temperature offshore of the Jet is warming faster than onshore of the Jet, which is consistent with other studies of warming rates on the MAB (Chen et al., 2020). Using the thermal wind equations, assuming that the salinity gradients have not changed and a depth scale of 80 m for the Shelfbreak Jet, the change in average Shelfbreak Jet velocities due to the changing temperature gradient is a reduction in the Shelfbreak Jet velocity of 0.01 m s^{-1}. While this does not account entirely for the decreasing velocity trend over 25 years, it suggests that the warming of the Slope Sea is reducing the velocity of the Shelfbreak Jet.

5. Conclusion

The data collected by the *CMV* Oleander have provided a unique opportunity to observe the Shelfbreak Jet over the span of two and half decades. Over the 25 years, we use 1,362 velocity transects, allowing us to resolve timescales from individual events, to monthly variability, to long-term variability. We focus on analyzing patterns in the velocity data, looking at time periods when the Shelfbreak Jet is shifted in position, or when it does not exist in an ADCP transect. These analyses are able to capture the composite impact of individual events on the Shelfbreak Jet, as well as look at variability that exists within and between years.

Throughout our results, we have demonstrated that the signature of Warm Core Rings is present during many phases of Shelfbreak Jet variability. Both when the Shelfbreak Jet is found onshore of its mean position, as well as during time periods when the Shelfbreak Jet cannot be identified, we see ADCP velocity, and satellite SST and SSH signals that would suggest Warm Core Ring influence. Additionally, the most distinct Warm Core Rings in the velocity data occur during time periods that are anomalously warm on the shelf, suggesting that Warm Core Rings are influencing both the velocity and temperature structure at the shelf break and on the shelf. With increasing numbers of Warm Core Rings since 2000, understanding how these impact the shelf break is growing in importance (Gangopadhyay et al., 2019).

We have found that the Shelfbreak Jet is not a permanent feature, but without simultaneous measurements of temperature and salinity with depth, it is unknown to us how the Shelfbreak Front is impacted during time periods when the Shelfbreak Jet is not identified. If the same processes that shutdown the Shelfbreak Jet also disrupt the Shelfbreak Front, then the nonpermanence of these features is crucially important. When these features do not exist, there would be no frontal convergence near the bottom (Houghton & Visbeck, 1998). Without the convergence, the upwelling of nutrients leading the shelf break to be a productive ecological region would be temporarily reduced. Due to limitations of the shipboard ADCPs in taking measurements near the bottom, we are not able to resolve this convergence and thus require additional measurements to resolve the relationship between the frontal upwelling and the shutdown of the Shelfbreak Jet.

Average shelf temperatures are also heightened during time periods with a weaker Shelfbreak Jet. Both Warm Core Rings and upstream advective processes are likely influencing the temperature on the shelf. The relative contribution of Warm Core Rings and along-shelf advection on both the shelf temperature and velocity structure remain a question that is of import to study. The shelf break region has economically significant fisheries that are potentially vulnerable to ocean warming and changes in shelf break exchange processes (e.g., Gawarkiewicz et al., 2018; Hare et al., 2016). Recent temperature variability has also influenced the stock distribution of fisheries in the Northeast United States, with certain species recruitment being correlated to temperature (Friedland, 2012; Gawarkiewicz et al., 2013; Miller et al., 2016). Understanding the connection between the temperature variability and Shelfbreak Jet system could be important to management of living marine resources in the shelf break region.

We have diagnosed the structure of the mean velocities over the New Jersey shelf break, as well as the mean Shelfbreak Jet velocities. From our climatologies, we have shown that both the structure of the Shelfbreak Jet and the maximum jet velocity show large seasonal variability. The jet undergoes time periods where it is shifted onshore and offshore, as well as when it can be identified in a velocity transect and not. These variations appear to be forced in part by individual events like Warm Core Rings. Larger-scale processes may

also be impacting the Shelfbreak Jet such as upstream advective flows from the Labrador Sea. The Shelfbreak Jet undergoes variability on timescales of days to decades, and in an ever changing system, it is important to understand the drivers of the variability.

Data Availability Statement

ADCP data product is available at https://doi.org/10.5281/zenodo.3935983, XBT data product is available at https://doi.org/10.5281/zenodo.3967332, raw *CMV* Oleander data are available at http://oleander.bios.edu/data/, altimetry data are available at https://marine.copernicus.eu/, and sea surface temperature data are available at from the NCDC website (https://www.ncdc.noaa.gov/oisst).

Acknowledgments
J. F. and M. A. were supported by NSF OCE-1634094 and OCE-1924041. G. G was supported by NSF OCE-1851261.

References

Andres, M. (2016). On the recent destabilization of the Gulf Stream path downstream of Cape Hatteras. *Geophysical Research Letters*, *43*, 9836–9842. https://doi.org/10.1002/2016GL069966

Bane, J. M., Brown, O. B., Evans, R. H., & Hamilton, P. (1988). Gulf Stream remote forcing of shelfbreak currents in the Mid-Atlantic Bight. *Geophysical Research Letters*, *15*(5), 405–407.

Beardsley, R. C., Chapman, D. C., Brink, K. H., Ramp, S. R., & Schlitz, R. (1985). The Nantucket Shoals Flux Experiment (NSFE79). Part I: A basic description of the current and temperature variability. *Journal of Physical Oceanography*, *15*(6), 713–748. https://doi.org/10.1175/1520-0485(1985)015<0713:TNSFEP>2.0.CO;2

Chelton, D. B., Schlax, M. G., & Samelson, R. M. (2011). Global observations of nonlinear mesoscale eddies. *Progress in Oceanography*, *91*(2), 167–216. https://doi.org/10.1016/j.pocean.2011.01.002

Chen, K., Gawarkiewicz, G. G., Lentz, S. J., & Bane, J. M. (2014). Diagnosing the warming of the Northeastern US Coastal Ocean in 2012: A linkage between the atmospheric jet stream variability and ocean response. *Journal of Geophysical Research: Oceans*, *119*, 218–227. https://doi.org/10.1002/2013JC009393

Chen, Z., Kwon, Y. O., Chen, K., Fratantoni, P., Gawarkiewicz, G., & Joyce, T. M. (2020). Long-term SST variability on the northwest atlantic continental shelf and slope. *Geophysical Research Letters*, *47*, e2019GL085455. https://doi.org/10.1029/2019GL085455

Egbert, G. D., & Erofeeva, S. Y. (2002). Efficient inverse modeling of barotropic ocean tides. *Journal of Atmospheric and Oceanic Technology*, *19*(2), 183–204. https://doi.org/10.1175/1520-0426(2002)019<0183:EIMOBO>2.0.CO;2

Flagg, C. N., Dunn, M., Wang, D. P., Rossby, H. T., & Benway, R. L. (2006). A study of the currents of the outer shelf and upper slope from a decade of shipboard ADCP observations in the Middle Atlantic Bight. *Journal of Geophysical Research*, *111*, C06003. https://doi.org/10.1029/2005JC003116

Flagg, C. N., Schwartze, G., Gottlieb, E., & Rossby, T. (1998). Operating an acoustic Doppler current profiler aboard a container vessel. *Journal of Atmospheric and Oceanic Technology*, *15*(1), 257–271. https://doi.org/10.1175/1520-0426(1998)015<0257:OAADCP>2.0.CO;2

Forsyth, J. S. T., Andres, M., & Gawarkiewicz, G. G. (2015). Recent accelerated warming of the continental shelf off New Jersey: Observations from the CMVOleander expendable bathythermograph line. *Journal of Geophysical Research: Oceans*, *120*, 2370–2384. https://doi.org/10.1002/2014JC010516

Fratantoni, P. S., & Pickart, R. S. (2003). Variability of the shelf break jet in the Middle Atlantic Bight: Internally or externally forced? *Journal of Geophysical Research*, *108*(C5), 3166. https://doi.org/10.1029/2002JC001326

Fratantoni, P. S., & Pickart, R. S. (2007). The Western North Atlantic shelfbreak current system in summer. *Journal of Physical Oceanography*, *37*(10), 2509–2533. https://doi.org/10.1175/JPO3123.1

Fratantoni, P. S., Pickart, R. S., Torres, D. J., & Scotti, A. (2001). Mean structure and dynamics of the shelfbreak jet in the Middle Atlantic Bight during fall and winter. *Journal of Physical Oceanography*, *31*(8), 2135–2156. https://doi.org/10.1175/1520-0485(2001)031<2135:MSADOT>2.0.CO;2

Friedland, K. (2012). Ecosystem advisory for the northeast shelf large marine ecosystem. Advis. 2012 No 2.

Gangopadhyay, A., Gawarkiewicz, G., Silva, E. N. S., Monim, M., & Clark, J. (2019). An observed regime shift in the formation of warm core rings from the Gulf Stream. *Scientific Reports*, *9*, 12319. https://doi.org/10.1038/s41598-019-48661-9

Gawarkiewicz, G., Bahr, F., Beardsley, R. C., & Brink, K. H. (2001). Interaction of a slope eddy with the shelfbreak front in the Middle Atlantic Bight. *Journal of Physical Oceanography*, *31*(9), 2783–2796. https://doi.org/10.1175/1520-0485(2001)031<2783:IOASEW>2.0.CO;2

Gawarkiewicz, G., Brink, K. H., Bahr, F., Beardsley, R. C., Caruso, M., Lynch, J. F., & Chiu, C. S. (2004). A large-amplitude meander of the shelfbreak front during summer south of New England: Observations from the Shelfbreak PRIMER experiment. *Journal of Geophysical Research*, *109*, C03006. https://doi.org/10.1029/2002JC001468

Gawarkiewicz, G., Chen, K., Forsyth, J., Bahr, F., Mercer, A. M., Ellertson, A., & Han, L. (2019). Characteristics of an advective marine heatwave in the Middle Atlantic Bight in early 2017. *Frontiers in Marine Science*, *6*, 712. https://doi.org/10.3389/fmars.2019.00712

Gawarkiewicz, G., Ferdelman, T. G., Church, T. M., & Luther, G. W. (1996). Shelfbreak frontal structure on the continental shelf north of Cape Hatteras. *Continental Shelf Research*, *16*(14), 1751–1773. https://doi.org/10.1016/0278-4343(96)00014-3

Gawarkiewicz, G., Lawson, G., Petruny-Parker, M., Fratantoni, P., & Hare, J. (2013). The shelf break ecosystem off the Northeastern United States: Current issues and recommended research directions. *Cooperative Institute for the North Atlantic Region, Woods Hole, Mass*. Available at http://cinar.org/fileserver.do, 29.

Gawarkiewicz, G., Todd, R. E., Zhang, W., Partida, J., Gangopadhyay, A., Monim, M. U. H., & Dent, M. (2018). The changing nature of shelf-break exchange revealed by the ooi pioneer array. *Oceanography*, *31*(1), 60–70.

Hare, J. A., Morrison, W. E., Nelson, M. W., Stachura, M. M., Teeters, E. J., Griffis, R. B., & Griswold, C. A. (2016). A vulnerability assessment of fish and invertebrates to climate change on the Northeast U.S. continental shelf. *PLOS ONE*, *11*(2), 1–30. https://doi.org/10.1371/journal.pone.0146756

Houghton, R. W., & Visbeck, M. (1998). Upwelling and convergence in the Middle Atlantic Bight Shelfbreak Front. *Geophysical Research Letters*, *25*(15), 2765–2768. https://doi.org/10.1029/98GL02105

Linder, C. A., & Gawarkiewicz, G. (1998). A climatology of the shelfbreak front in the Middle Atlantic Bight. *Journal of Geophysical Research*, *103*(C9), 18,405–18,423. https://doi.org/10.1029/98JC01438

Loder, J. W., Petrie, B., & Gawarkiewicz, G. (1998). The coastal ocean off northeastern North America: A large-scale view. *The Sea*, *11*, 105–133.

Miller, T. J., Hare, J. A., & Alade, L. A. (2016). A state-space approach to incorporating environmental effects on recruitment in an age-structured assessment model with an application to southern New England yellowtail flounder. *Canadian Journal of Fisheries and Aquatic Sciences*, *73*(8), 1261–1270. https://doi.org/10.1139/cjfas-2015-0339

Peña-Molino, B., & Joyce, T. M. (2008). Variability in the Slope Water and its relation to the Gulf Stream path. *Geophysical Research Letters*, *35*, L03606. https://doi.org/10.1029/2007GL032183

Reynolds, R. W., Smith, T. M., Liu, C., Chelton, D. B., Casey, K. S., & Schlax, M. G. (2007). Daily high-resolution-blended analyses for sea surface temperature. *Journal of Climate*, *20*(22), 5473–5496. https://doi.org/10.1175/2007JCLI1824.1

Rossby, T., & Benway, R. L. (2000). Slow variations in mean path of the Gulf Stream east of Cape Hatteras. *Geophysical Research Letters*, *27*(1), 117–120. https://doi.org/10.1029/1999GL002356

Zhang, W. G., & Gawarkiewicz, G. G. (2015). Dynamics of the direct intrusion of Gulf Stream ring water onto the Mid-Atlantic Bight shelf. *Geophysical Research Letters*, *42*, 7687–7695. https://doi.org/10.1002/2015GL065530